AVE Trends in Intelligent Health Letters

A Breakthrough in Cervical Cancer Detection Using AEO-Infused Enhanced DenseNet Classification

B. Santosh Kumar[1,*], Thirumalraj Karthikeyan[2], R. J. Anandhi[3], S. Venkatasubramanian[4], Chou Yi Hsu[5]

[1]Department of Computer Science and Engineering, New Horizon College of Engineering, Bengaluru, Karnataka, India.
[2]Department of Artificial Intelligence, Quest Technologies, Trichy Research Labs, Tiruchirappalli, Tamil Nadu, India.
[3]Department of Information Science and Engineering, New Horizon College of Engineering, Bengaluru, Karnataka, India.
[4]Department of Computer Science and Business Systems, Saranathan College of Engineering, Trichy, Tamil Nadu, India.
[5]Department of Pharmacy, Chia Nan University of Pharmacy and Science, Rende, Tainan, Taiwan.
skumars1803@gmail.com[1], thirumalraj.k@gmail.com[2], rjanandhi@hotmail.com[3], veeyes@saranathan.ac.in[4], joyhsu@yuanangroup.com.tw[5]

*Corresponding author

Abstract: Among women, cervical cancer is a widespread and treatable cancer that is a long-term disease. The most effective method for quickly diagnosing cervical cancer is Pap smear testing. The approach used to detect cervical cancer focuses on using new image-processing techniques and better classification parameters. The process is initialised with Gabor preprocessing, which improves crucial features in cervical images using the SIPaKMeD dataset. GhostNet uses Artificial Ecosystem-based Optimisation (AEO) to hyperparameter-tune and ensure better model performance. The classification phase is empowered by an Enhanced DenseNet architecture, specifically AdaBound-Squeeze and Excitation-DenseNet. It integrates adaptive optimisation and spatial squeeze-and-excitation mechanisms for improved learning and feature representation. The proposed framework achieves 99.41% accuracy, 99.41% precision, 99.43% recall, and 99.45% F-score, which are better results than those of other existing models. The method has been proposed, tested, and its efficacy has been confirmed. The technique can be applied in clinical settings to help detect cervical cancer early.

Keywords: Gabor Filter; Ghost Network; Squeeze and Excitation; Dense Network; Artificial Ecosystem Optimisation; Cancer Diagnoses; Cervical Cancer; Identification and Treatment; Health Care Services.

Cite as: B. S. Kumar, T. Karthikeyan, R. J. Anandhi, S. Venkatasubramanian, and C. Y. Hsu, "A Breakthrough in Cervical Cancer Detection Using AEO-Infused Enhanced DenseNet Classification," *AVE Trends in Intelligent Health Letters*, vol. 2, no. 3, pp. 150 –162, 2025.

Journal Homepage: https://avepubs.com/user/journals/details/ATIHL

Received on: 20/10/2024, **Revised on:** 30/01/2025, **Accepted on:** 13/04/2025, **Published on:** 07/09/2025

DOI: https://doi.org/10.64091/ATIHL.2025.000173

1. Introduction

With 6.6% of all female cancer diagnoses in 2018 were cervical cancer, making it still the world's fourth most common malignant tumour in women [1]. Cervical cancer claims the lives of fewer than 300,000 women worldwide each year, but more than 500,000 women receive a diagnosis [2]. About 604,000 women received a cervical cancer diagnosis in 2020. 2020 saw about 90% of Countries with low and middle incomes account for about 342,000 of the deaths from cervical cancer [3]. Africa has the highest rate of cervical cancer cases, accounting for over 85% of cases, which occur in developing nations. These

nations have higher cancer mortality rates [4]. This is brought on by limited access to healthcare and a lack of understanding about the illness. Conversely, developed nations have policies in place that enable the use of precise and effective screening instruments, allowing precancerous lesions to be identified and treated early. Early identification and treatment of premalignant lesions is known to halt the progression of cervical cancer in nearly 90% of cases [5]. Consequently, it's critical to detect cervical cancer early on. Cervical cancer has several challenges that appear to be diagnostic, mainly because of multiple factors. A hurdle in the pathway to efficient, early diagnosis is limited access to health care services in some areas [6]. Moreover, due to cultural barriers and little knowledge about the significance of cervical cancer screenings, there is a delay in its diagnosis. Because cervical cancer does not exhibit any particular symptoms in its early stages, it becomes difficult to detect [7].

In some scenarios, the Pap smear can yield false positives or negatives, which can affect the precision of the outcomes, since the test provides only limited outcomes; the results can't be relied upon. In certain areas where resources are scarce, healthcare professionals and advanced diagnostic technologies are hard to find [8]. Another aspect that needs to be addressed is making healthcare equitable and educating the public about its importance in their lives. In addition to cutting-edge deep learning (DL) methods that automatically identify deep features in medical images, modern CAD systems are being developed. DL methods can be applied to a range of image characteristics and attributes [9]. To convert raw image data into discriminative features, DL-based methods can be combined with conventional feature-extraction methods. Conversely, DL-based algorithms outperform traditional methods in classification problems, despite research suggesting that combining traditional handcrafted features with deep learning features could enhance diagnostic performance [10]. Convolutional neural networks (CNNs) are among the DL architectures that have achieved notable success in a variety of health and medical imaging applications over the past few years, particularly in computed tomography scanning, histopathology, mammography, magnetic resonance imaging, fundus imaging, and facial images [11]. The remarkable success of CNNs across various medical and health domains has led to their use in numerous CAD models for cervical cancer diagnosis [12]. CNN models require substantial data to prevent overfitting and erroneous generalisations [13].

1.1. Motivation

To improve patient outcomes and effectively remedy the issue, it is important to detect cervical cancer in its early stages. This study will introduce advanced changes to the classification and diagnosis of cervical cancer, enhancing effectiveness and precision. The diagnostic techniques will not only be improved but will also positively impact overall health standards for females, indeed. This study aims to provide healthcare professionals with a well-established technique for identifying the disease in its early stages. This work is the cornerstone in controlling the global fight against cervical cancer, because it reduces the number of advanced cases and ultimately saves many lives.

1.2. Main Contributions

- **Effective Preprocessing with Gabor Filtering:** This process uses the Gabor filter to extract the most informative features from pap smear images. To identify patterns specific to cervical cancer, it is important to improve how a particular feature is represented, and this is the first step.
- **Utilisation of AEO-GhostNet for Feature Extraction:** A GhostNet has been incorporated into the study to extract relevant features and capture the most relevant information from cervical images. Through Artificial Ecosystem optimisation (AEO), fine-tuning values improve. This step can handle subsequent processes more accurately because it uses a richer feature set.
- **Empowerment of Classification with Enhanced DenseNet:** The enhanced network for phase classification is AdaBound-Squeeze, a DenseNet model. Regarding cervical cancer detection, spatial squeeze-and-excitation functions and adaptive optimisation techniques help produce a better feature set.

2. Related Works

The article by Fekri-Ershad and Alsaffar [14] presented a CAD model built on feature extraction across multiple domains rather than a single domain. It is simpler than current methods because it does not require a pre-segmentation step. Unlike current CADs, which use a single DL model with many parameters and layers to acquire high-level spatial deep features, this CAD uses three compact DL models. Additionally, unlike most existing CADs, it provides a more accurate representation of features linked to cervical cancer by retrieving several statistical and textural descriptors from various domains, including the spatial and time-frequency domains. It examines how each set of carefully chosen characteristics affects diagnostic precision, both individually and in combination. After that, it examines the effects of merging the manually created features across the DL feature sets offered by each CNN. Lastly, it examines the impact of combining several DL features with various handcrafted features via principal component analysis to determine how the combined handcrafted features affect classification outcomes across the entire set of DL features. The proposed CAD's quartic SVM achieved 100% accuracy with just 35 principal

components. The performance of the outlined CAD demonstrates that diagnostic accuracy can be increased by combining multiple DL features with a large number of manually created descriptors from various domains.

In the study by Karamti et al. [15], a combination method was used that completely separates the feature extraction step from the classification stage, with an overall framework derived from a machine learning approach. Deep networks are employed, nevertheless, in the feature extraction stage. This work presents an MLP neural network, which is a deep feature-fed multi-layer perceptron. These four novel concepts alter the total number of neurons in the hidden layer. Two other deep networks used as feedforward layers are ResNet-34, ResNet-50, and VGG-19. Following through a flattened layer, the outputs feed the MLP as presented, eliminating the layers associated with the classification phase from these two CNN networks. The Adam optimiser is used to train both CNNs on similar images to increase performance. When tested on the Herlev benchmark database, the proposed method achieved 99.23% accuracy for the two-class case and 97.65% for the seven-class case. The study by Alsalatie et al. [16] proposed a high-accuracy automated cervical cancer prediction system that effectively handles missing values using SMOTE. In the proposed system, three machine learning models are combined into a stacked ensemble voting classifier. To handle missing values, the model for a stacked ensemble voting classifier uses KNN Imputer and SMOTE up-sampling. Using SMOTE features imputed by KNN, the suggested model attains 99.99% F1 score, 99.99% accuracy, 99.99% precision, and 99.99% recall.

The study by Hamdi et al. [17] effectively uses feature weighting to develop a computer-aided diagnostic system for cervical cancer. Two new evolutionary algorithms, Ant Lion Optimisation (ALO) and Particle Swarm Optimisation (PSO), are used in the optimisation process. In conclusion, this study employs two machine learning algorithms for classification: the support vector machine and the random forest. When using the PSO algorithm, the SVM classifier outperformed the RF, achieving 98.9% accuracy in the same area and 99.5% across seven categories. The study by Kalbhor et al. [18] aims to develop criteria to detect epithelial cervical cancer cells earlier using automated whole-slide image datasets. A substantial number of computer systems have been advanced so that the progression of cervical cancer can be identified by looking at Whole Slide Imaging (WSI) images. To ensure that the edges of low-contrast cells were visible, the WSI images were carefully adjusted. Next, the Active Contour Algorithm was applied to parse and segment the remaining image into the intended cells. To test the WSI images, a hybrid solution has been proposed, including support vector machines (SVMs), random forests (RFs), and deep learning algorithms such as ResNet50, VGG19, and GoogLeNet. The basis for this research is the ACA algorithm. Support Vector Machine and Random Forest algorithms are used in a hybrid approach that combines several machine learning models, including ResNet50-VGG19, ResNet50-GoogLeNet, and VGG19-GoogLeNet, to diagnose digital whole-slide images. The models' performance is heavily dependent on the DL models, as evidenced by the results.

This study is innovative because it utilises a hybrid method to diagnose WSI images from two or more models. It has been analysed how well RF and SVM use the features provided by the deep learning models. When using ResNet50 and VGG19 features, the RF network achieved sensitivities of 97.4%, 99%, and 99.6%, and specificities of 99.2%, 99%, and 99.6%, respectively, with an AUC of 98.75%. In the paper by Kavitha et al. [19], the feature extraction and classification methods differ, and, according to my supervisor's opinion, they are considered state of the art. AlexNet, ResNet-18, ResNet-50, and GoogLeNet are the most well-known pre-trained deep learning models and are widely employed in real-world applications. SIPaKMeD and Herlev were benchmark datasets used in the experimentation. The Resnet-50 fine-tuned architecture achieves 95.33% classification accuracy, the highest, whereas AlexNet ranks second on the SIPaKMeD dataset. Benefiting from fuzzy min-max neural networks, the proposed model leverages the properties of classifiers highlighted in the literature, thereby improving accuracy. The article by Alquran et al. [20] explains how to improve pictures using Brightness Preserving Dynamic Fuzzy Histogram Equalisation. The proper region of interest is found, and components are divided by employing the fuzzy c-means technique. The fuzzy c-means technique is used to segment images and determine the relevant area of interest. The feature selection algorithm, or ACO algorithm, is the name given to it. From there, the CNN, MLP, and ANN algorithms are used for classification.

2.1. Research Gaps

Fekri-Ershad and Alsaffar [14] cervical cancer classification through the CAD model is unmatched. However, efforts are needed to expand its scalability and validate its clinical applications. Although the Karamti et al. [15] technique has demonstrated high performance, further studies are needed to ensure its stability and generalizability across different practice settings. The classifiers in Alsalatie et al. [16] demonstrate exceptional results. To validate whether these classifiers can generalise to larger, broader datasets, more studies are needed, as in the study by Hamdi et al. [17]. Even though feature-weighted diagnosis systems have been shown to provide improved outcomes, the extent to which this approach can be utilised in demographically diverse patient cohorts, and its implications, remain unclear in Kalbhor et al. [18]. The image analysis models in WSI are innovative, but they need to be validated in additional research studies to demonstrate their promise. There is potential in Kavitha et al.'s [19] new hybrid technique. However, further research is required to confirm its performance

compared to existing techniques. The effectiveness of the Alquran et al. [20] proposed technique needs further evaluation in clinical scenarios, such as its diagnostic accuracy, to be determined.

3. Proposed Methodology

Figure 1 illustrates the workflow of the proposed method in cervical cancer detection.

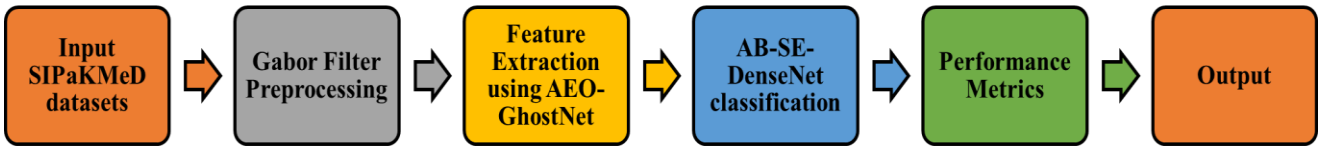

Figure 1: Block diagram

3.1. Dataset Description

SIPaKMeD datasets were used to acquire images for multi-cell classification [21]. In the multi-cell dataset, 966 images were included, and 4049 cells were cropped from them.

Table 1: Description of five cell classes derived from the SIPaKMeD (multi-cell) dataset

Class	Number of Images	Number of Cells
Normal Class		
1. Superficial-Intermediate Cells	126	831
2. Parabasal Cells	108	787
Benign Cell		
3. Metaplastic Cells	271	793
Abnormal Cells		
4. Dyskeratotic Cells	223	813
5. Koilocytotic Cells	238	825
Total	966	4049

The three stages of cells, normal, benign, and abnormal, should be noted. The cells were classified into five types: parabasal cells, koilocytotic cells, metaplastic cells, superficial–mediate cells, and dyskeratotic cells. Every dataset's details have been compiled in Table 1 [20]. Table 1 and Figure 2 illustrate a Pap smear from the SIPaKMeD dataset.

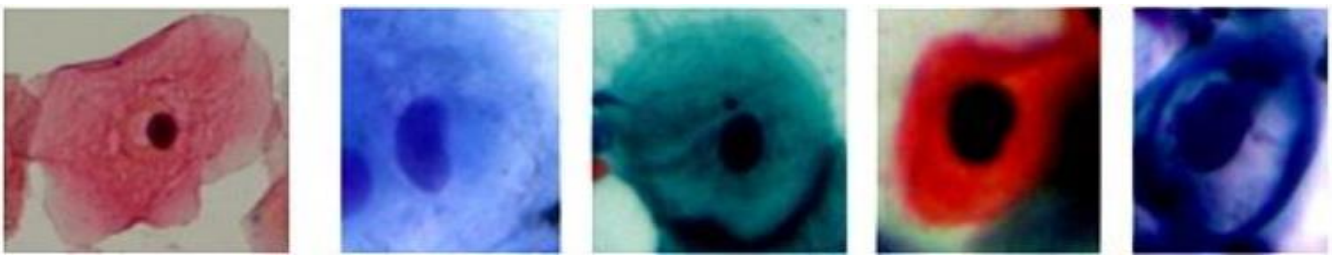

Figure 2: Example images from each class: (a) superficial, (b) parabasal, (c) metaplastic, (d) dyskeratotic, (e) koilocytotic

3.2. Pre-Processing with Gabor Filter

The GF technique is used in the first stage to prepare the pictures. The impulse response of this linear filter is the result of multiplying a Gaussian function by a sinusoidal function. They operate almost exactly like a passband. The main advantage of displaying that is the Gaussian envelope, in contrast to the sinusoidal function, which is precisely localised in the frequency domain and completely delocalized in the spatial domain (covering the entire space). There are two locations for the Gabor function: the spatial and frequency domains [22]. As a result, this function is ideal for signal representation in these fields. A 2D bandpass filter, Gabor preserves the original image's address and reduces noise when given a frequency and direction.

3.3. Feature Extraction Using the AEO-Ghostnet Model

3.3.1. Ghostnet Model

Using the GhostNet model yields a collection of feature vectors. The GhostNet model effectively gathers unwanted data from the network and eliminates features based on a set of parameters [23]. The standard convolutional function is reduced to two-step operations by the GhostNet component. The standard convolutional function is a first step, but it reduces the use of convolutional kernels. A simple linear function is used in the secondary stage to produce redundant mapping features. After the input mapping feature's dimensionality is $D_F x D_F x M$, the standard convolutional kernel's convolutional kernel is $D_k x D_k x N$, and the calculation amount is $D_k x D_k x M x D_F x D_F x N$. The GhostConv element's initial stage assumes that the quantity of processing and the possibility of producing m mapping features are $D_k x D_k x M x D_F x D_F x m$. To guarantee an output comparable in size to a single feature map, the compact linear function was used; the result of the primary stage's convolution was the GhostConv element's secondary stage, a typical convolutional output, as demonstrated by equation (1):

$$y_{ij} = \phi_{ij}(y_i'), \forall_i = 1, \cdots, m; j = 1, \cdots, s \quad (1)$$

whereas ϕ_{ij} symbolises a linear process, y_i' implies the i^{th} mapping feature, and y_{ij} stands for the j^{th} mapping feature obtained using a linear procedure of the i^{th} mapping feature. The GhostConv model receives N features for output mapping, where N = mxs. The computational resource-handling $s - 1$ linear conversion is completed; thus, the GhostConv model's computing count can be $D_K x D_K x M x D_F x D_F x m + (s-1) x D_K x D_K x D_F x D_F$. Next, the following is the expression for GhostConv's computation relationship with conventional convolutional modules:

$$\frac{D_K x D_K x M x D_F x D_F x N}{D_K x D_K x M x D_F x D_F x m + (s-1) x D_K x D_K x D_F x D_F} \approx s \quad (2)$$

Equation (2) indicates that convolutions are typically s times larger in the computation than the GhostConv element. Because of this, the GhostNet model was developed with the expectation that GhostNet-Block could significantly reduce the number of computations and network parameters.

3.3.2. Hyperparameter Tuning Using AEO

AEO, or Artificial Ecosystem-based Optimisation, is a recently proposed algorithm that is used in this paper for hyperparameter tuning of GhostNet [24]. It draws inspiration from the way energy flows in the Earth's biological system. This kind of mechanism mimics the decomposition, consumption, and production processes of living things. Any green plant that uses the process of photosynthesis to obtain its food can generally be considered a producer. In this process, known as photosynthesis, interactions between carbon dioxide and water, which occur in the absence of sunlight, produce sugar, oxygen, and glucose. Plants then use this sugar to create their fruits, leaves, roots, and wood. Thus, the producers provided the necessary food for the herbivore and omnivore consumers. Given that they are animals and cannot produce their own food, consumers can only eat food that producers or other consumers provide. There are three different kinds of consumers in nature: herbivores, omnivores, and carnivores. Herbivores are animals that only consume plants, or producers; omnivores, on the other hand, are animals that can consume both producers and other animals. Furthermore, these creatures that exclusively consume other animals are known as carnivores. Decomposers are organisms that consume the waste products of living things, such as dead plants and animals. The majority of bacteria and fungi are decomposers; they break down the remains of dead organisms and transform them into simple molecules such as carbon dioxide, water, and minerals. Producers then absorb these forms of energy and use photosynthesis to produce sugar. These behaviours can be mathematically modelled so that, during the optimisation process, the production action can regulate the trade-off between exploitation and exploration. The consumer controls the search space during the decomposition action, which can be terminated by removing the intensification. Through this system, plants obtain nutrients from carbon dioxide, water, sunlight, and bacteria and fungi that break down nutrients. This is a summary of the update process:

- **Production Process:** The producer position is chosen at random, and the corresponding producer is the worst, as in Jiang et al. [25]. Nonetheless, the following equations (3)–(5) can be used to model the optimal solution as represented by the decomposer:

$$X_1(t+1) = (1-d)X_n(t) + d \cdot X_{rand}(t) \quad (3)$$

$$d = \left(1 - \frac{t}{T_{max}}\right) \text{rand}_1 \quad (4)$$

$$X_{rand}(t) = rand_2() \cdot (ub - lb) + lb \quad (5)$$

where t and T_{ma} are, respectively, the number of iterations completed and the current iteration. The search space's upper and lower boundaries are represented by the variables ub and lb.. rand d_1 and $rand_2$ are variables that are arbitrary in the range (0,1), where d is the parameter for weight. X_{rand} (t) gives away a solution that the search space produced at random:

- **Consumption process:** In this process, the first user feeds on a producer or on the other user who is less energetic. The three user groups—omnivores, vegetarians or herbivores, and carnivores—each have a mechanism for updating their status in the following ways.

(a) The locations of the herbivores can be updated solely in consideration of the producers:

$$X_i(t+1) = X_i(t) + K \cdot (X_i(t) - X_1(t)) \quad (6)$$

where X_1 Equation (7) uses the Levy flight to determine the producer's location, where K is a parameter for consumption, and equation (6) represents the producer's location:

$$K = \frac{1}{2}\frac{u}{v},\ u \in Norm(0,1), v \in Norm(0,1) \quad (7)$$

Wherein the variable Norm (0,1) is produced using the zero mean of the normal distribution and unit variance. (b) The arbitrary consumer with multiple energy levels and an index (l) operates the carnivores' update process. Equations (8) and (9) can be used to model this process as follows:

$$X_i(t+1) = X_i(t) + K \cdot (X_i(t) - X_l(t)) \quad (8)$$

$$l = randi([2i-1]), i = 3, \ldots, N \quad (9)$$

Where randi $[a, b]$ is a function that produces random integer numbers in $[a, b]$. (c) Omnivores' position updates are reliant on the producer and an energy-index-high randomly chosen consumer (l), as stated in the following framework:

$$X_i(t+1) = X_i(t) + K \cdot \left(rand_3 \cdot (X_i(t) - X_1(t))\right) + (1 - rand_3) \cdot (X_i(t) - X_l(t)),$$
$$l = randi([2i-1]), i = 3, \ldots, N \quad (10)$$

- **Decomposition process:** This is the final stage of the biological system, in which all agents die, and the remaining components are divided. This step, which is the utilisation of AEO, is derived from equations (11)-(14) as stated in Jiang et al. [25]:

$$X_i(t+1) = X_i(t) + D \cdot (e \cdot X_n(t) - h \cdot X_i(t)), i = 1, \ldots, N \quad (11)$$

$$D = 3u,\ u \in N(0,1) \quad (12)$$

$$e = rand_4 \cdot randi([1 \quad 2]) - 1 \quad (13)$$

$$h = 2 \cdot rand_4 - 1 \quad (14)$$

The parameter D represents the decomposition factor; h and e symbolise the weight parameters. rand $_4$ is a haphazard Figure distributed uniformly over $(0,1)$. The first algorithm provides the AEO steps. Furthermore, the AEO has several advantages over other MH techniques, such as not requiring parameter determination throughout the optimisation process. It also possesses a strong ability to strike a harmony between discovery and production, improving convergence and preventing getting stuck at local optima. As a result, it raises the quality.

3.4. Classification Using DenseNet

The DenseNet convolutional neural network was introduced in 2017. The dense internal block, or "Dense Block," is the primary structural component of the DenseNet network. The inner dense module is composed of 3×3 and 1×1 convolutional layers (Conv), batch normalisation (BN), and the ReLU activation function. Every neuron not only forms connections with its predecessor neurons but also with the neurons in front of it; in the case of L neurons in a dense block, these connections are L×(L+1)/2. Equation (15) shows the first layer's output in the following way:

$$X_l = H_l([x_0, x_1, \ldots, x_{l-1}]) \quad (15)$$

where H_l symbolises the layer's convolution operation l, and x_l symbolises the layer's output l:

- **BN:** ReLU stands for activation function; batch normalisation. Convolution layers, such as 1×1 and 3×3 convolution, are represented by the symbol Conv.

Usually, to avoid complex computations, a 1×1 convolutional layer, or bottleneck module, is included in the dense block to reduce the number of features. Transition layers are used to link adjacent dense blocks, reducing the network's total parameter count and boosting computational efficiency. The pooling that makes up the transition layer and the convolutional layers. The transition layer consists of a 2×2 AvgPooling layer and a convolutional layer.

3.4.1. SE Module

While the gradient disappearance issue is somewhat resolved when cervical cancer detection is performed with the DenseNet network, there is no connection-weight setting, and any two layers are connected via an equal-weighted output fusion. The output from the main road's upper layer should be utilised as a key processing object for each layer's input, starting with the lower layer's input. The proportion should decrease because of the combined output of earlier layers; however, some deeper layers may still use features extracted from earlier layers directly, and some transition layers produce many redundant features, which cause subsequent dense blocks to use the previous output features less frequently. This work proposes an adaptively weighted, densely connected convolutional neural network with unequal layers. The DenseNet network architecture gains the SE module. The weight-adaptive approach is used, with each channel's weight determined by the degree of dependence among feature channels to mitigate the effects of feature duplication and support the neural network's learning of critical feature information. The two activation mechanisms, completely interconnected levels, and fundamental structures of global average pooling are the main components of the SE module. Primarily split into excitation and squeeze operations. The compression operation reduces the number of parameters by compressing the characteristics. A map of C×H×W dimensions (W = width, H = height, and C = quantity of featured channels) is divided into C×1×1 features using special pooling layers. Furthermore, it won't alter the overall channel dimension. There is an input set if the size of the feature map input is C×H×W, $U = [u_1, u_2, \ldots, u_c]$Equation (16) represents the mapping relationship for the compression operation:

$$Z_c = Fsq(u_c) = \frac{1}{H \times W} \sum_{i=1}^{H} \sum_{j=1}^{W} u_c(i, j) \quad (16)$$

Where $c \in C, Zc$ denotes the global data from c feature maps, and Fsq denotes the process of squeezing. The sigmoid activation function and the full connection layer comprise the excitation operation. The full connection layer integrates all input characteristic data, and the input is mapped to the interval (0,1) using the sigmoid function. The incentive operation's mapping relationship is displayed as follows in Equation (17):

$$s = Fex(Z, W) = \sigma(g(Z, W)) = \sigma\big(W_2 \cdot \delta(W_1 \cdot Z)\big) \quad (17)$$

Wherein σ is the sigmoid's activation function, δ is the activation function of the ReLU, Fex is the mechanism of excitation, and W_1 and W_2 weight parameters that are relevant to the connection layer as a whole. Ultimately, after scaling and multiplying the input channel's weight by the channel feature's weight learned by the SE module, the process produces the fused feature by combining the original feature and the weight. This results in the network's input receiving fused features related to cervical diseases, reducing feature redundancy and boosting network performance. Fsq represents the SE module's data squeezing. Fex represents the SE module's excitation operation. Channel weights are multiplied by the scale.

3.4.2. AB-SE-DenseNet

The SE-DenseNet network is built using the SE module (as indicated in Table 2) and the DenseNet framework from Section 3.4. Using the SE module and global information, the network learns to accentuate positive traits while suppressing negative ones. This reduces the impact of DenseNet-caused feature redundancy, adjusts how feature channels adapt, and enhances network performance. With the dense network, a portion of the standard convolution is replaced by the depth-wise separation convolution. The corresponding channel convolution kernel in the input channel is convolved via the depth-wise convolution of the depth-wise separable convolution. Next, to integrate all feature maps and lower the total number of network parameters, the point convolution operation is employed. Table 2 displays the SE-DenseNet model's frame structure parameters.

Table 2: Model frame architecture of SE-DenseNet

Network	Parameter
SE Layer	Squeeze, Excitation
Input Layer	224 x 224 x 3
Convolution Layer	3 X 3 DwsConv
Classification Layer	7 X 7 global average pool Full layer
Dense Block 1	3 X 3 DwsConv} n
Transition Layer 2	1 x1 Conv 2x 2 average pool, stride2
Transition Layer 1	1 x 1 Conv 2 x 2 average pool, stride2
Dense Block 2	3 X 3 DwsConv} X n
SE Layer	Squeeze, Excitation
Dense Block 3	3 x3 DwsConv x n

There are several embedded locations for the SE module in DenseNet. Three distinct network models are presented in this paper: SE-DenseNet-1, SE-DenseNet-2, and SE-DenseNet-3. SemanticNet-1, SemanticNet-2, and SemanticNet-3 are these. The dense block of the DenseNet model contains the embedded SE module, thanks to SE-DenseNet-1, as well as the adjacent transition layer. The SE module is concurrently embedded in DenseNet's transition layer and dense block by SE-DenseNet-3. The AB-SE-DenseNet network is trained using the AdaBound algorithm, which dynamically adjusts the learning rate. Model fitting can be accelerated with AdaBound, which also improves model performance and learning rate.

4. Results and Discussion

4.1. Experimental Setup

This paper used the experimental environment setup shown in Table 3 to assess the method's performance.

Table 3: Configuration of the experimental environment

Operating system	64 Bit Windows 10
Graphics card	GTX1050Ti (4 GB)
Learning framework	Pytorch
Ram	16 GB
CPU	Intel i7-6700
Hard disk	1 TB

4.2. Performance Metrics

To assess a model's deep learning performance, an evaluation metric is a confusion matrix, along with the model's accuracy (Acc), precision (Pre), recall (Rec), and F1 score (F1). The accuracy rate is the percentage of samples correctly classified relative to the total number of samples. Stated differently, the accuracy rate is the ratio of accurately identified genuine samples to the total number of genuine samples. One definition of the ratio is the recall rate of properly categorised samples to all effectively classified samples. The weighted average of recall and precision is known as the F1 value. Formulae (18) through (21) provide the allometric computation. The quantities in these formulas represent the number of accurately predicted positive samples (TP) and the number of falsely predicted positive samples (FP). For every positive sample, the quantity of erroneous samples correctly predicted (TN) equals the quantity of erroneous samples incorrectly predicted (FN):

$$\text{Acc} = \frac{\text{TP+TN}}{\text{TP+TN+FP+FN}} \tag{18}$$

$$\text{Pre} = \frac{\text{TP}}{\text{TP+FP}} \tag{19}$$

$$\text{Rec} = \frac{\text{TP}}{\text{TP+FN}} \tag{20}$$

$$\text{F1} = \frac{2\text{TP}}{2\text{TP+FP+FN}} \tag{21}$$

Table 4: Classification analysis of various classes of cervical cancer

Classes	ACC	PRE	REC	F1
Superficial-Intermediate Cells	97.98	97.95	97.51	97.41
Parabasal Cells	97.48	97.62	97.26	97.34
Metaplastic Cells	97.88	98.33	97.99	97.84
Dyskeratotic Cells	99.41	97.03	98.03	98.63
Koilocytotic Cells	98.89	98.72	98.64	98.59

Table 4 and Figure 3 show that the proposed method for detecting cervical cancer performs well across different cell types. Superficial-Intermediate Cells are very accurate at 97.98%. They show strong and reliable ACC, REC, and F1 Scores of 97.95%, 97.51%, and 97.41%, respectively. Parabasal Cells also achieve an important ACC of 97.48%, along with good PRE, REC, and F1s of 97.62%, 97.26%, and 97.34%, respectively.

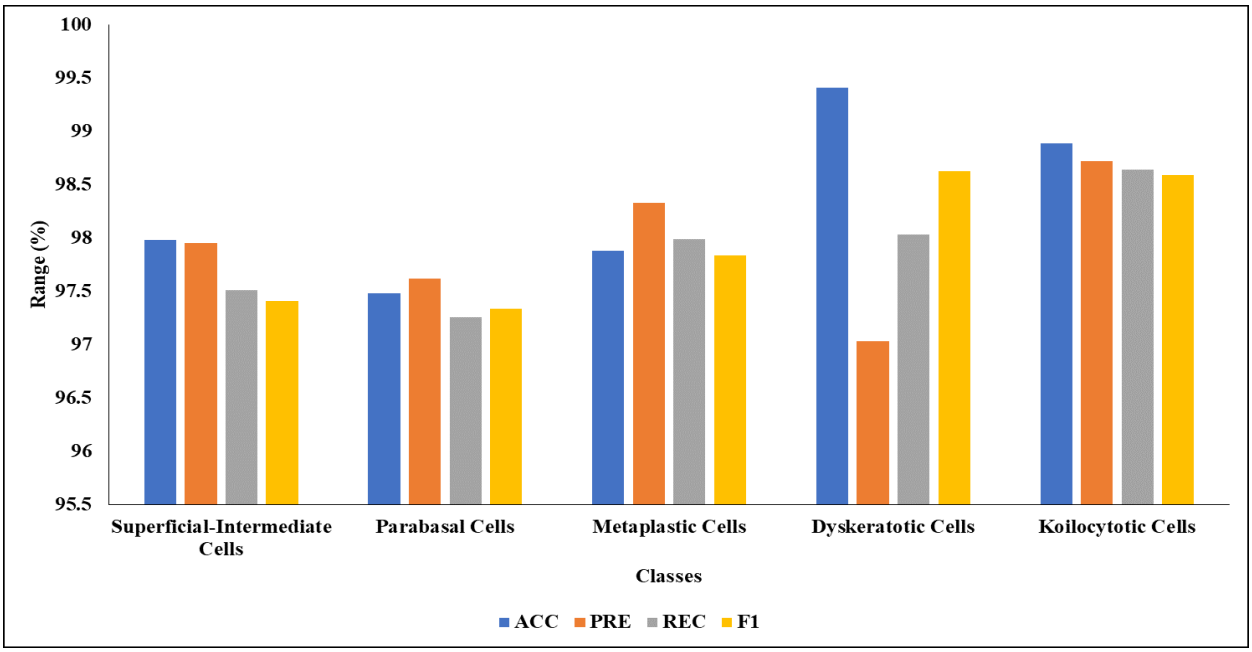

Figure 3: Various classes of cervical cancer analysis

Metaplastic Cells perform very well, with an ACC of 97.88%, and yield close matches, with PRE, REC, and F1 of 98.33%, 97.99%, and 97.84%, respectively. The results for Dyskeratotic Cells are very impressive. They have an ACC of 99.41%. The PRE, REC, and F1s are 97.03%, 98.03%, and 98.63%, respectively. Koilocytotic Cells show great performance with a success rate of 98.89%. They also have strong ACC, PRE, and REC scores of 98.72%, 98.64%, and 98.59%, respectively, and an F1 score of 98.59%. This framework works well and can be counted on for different types of cervical cells. It could be used in real medical settings to determine if someone has cervical cancer accurately.

Table 5: Classification analysis of various DL models with the proposed AB-SE-Densenet model

Models	ACC	PR	RC	F1
ResNet	91.60	93.16	91.34	92.14
VGG16	94.52	95.48	93.56	93.25
GoogLeNet	96.33	96.34	95.63	94.58
XceptionNet	97.64	97.66	97.57	96. 69
Proposed AB-SE-DenseNet Model	99.41	99.41	99.45	99.43

Looking at the different models of tests for cervical cancer from Table 5 and Figure 4 shows that they have different levels of success. ResNet achieves an ACC of 91.60%. It has strong matching PRE, REC, and F1 Scores of 93.16%, 91.34%, and 92.14%, respectively. The VGG16 model does better. It achieves 94.52% accuracy, along with PRE, REC, and F1 scores of 95.48%, 93.56%, and 93.25%, respectively.

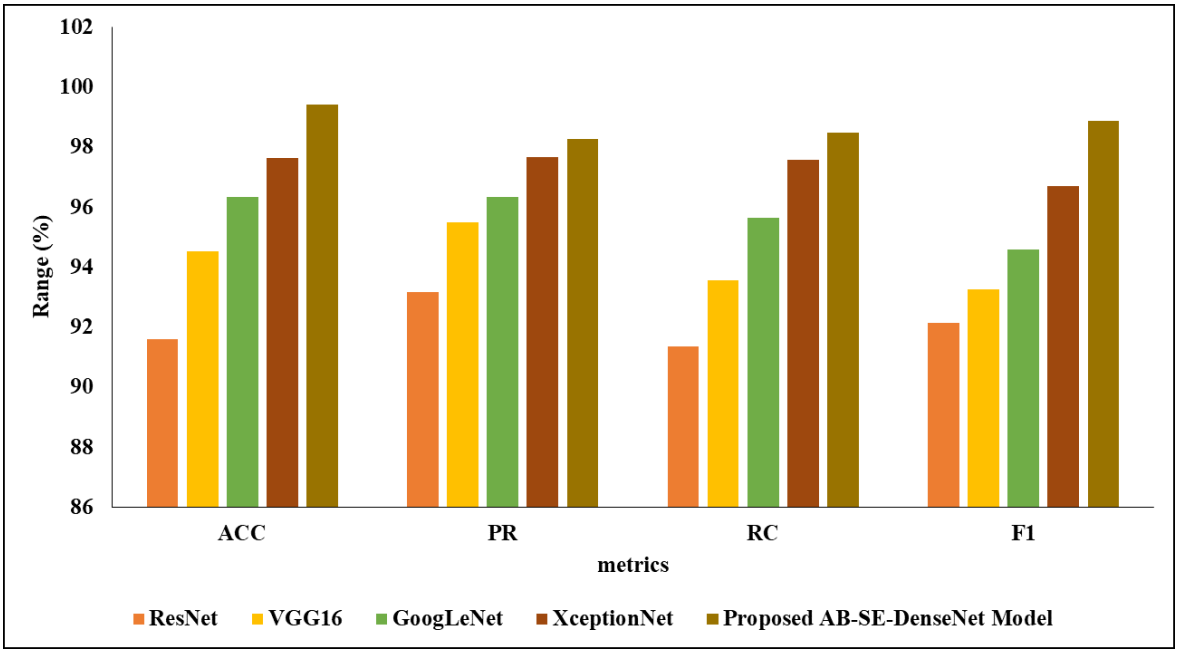

Figure 4: Classification analysis with different DL models

GoogLeNet improves further, achieving an ACC of 96.33%. It shows strong PRE, REC, and F1 Scores of 96.34%, 95.63%, and 94.58%, respectively. XceptionNet performs very well, achieving an ACC of 97.64%. It also shows good results for PRE, REC, and F1, with Scores of 97.66%, 97.57%, and 96.69%, respectively. Notably, the proposed AB-SE-DenseNet model performs best. It scores an impressive 99.41% and outperforms other methods on PRE, REC, and F1. These are 99.41%, 99.45%, and 99.43%, respectively. This shows that the suggested plan works well, suggesting it could make cervical cancer screening much more accurate and reliable than older methods such as ResNet, VGG16, GoogLeNet, and XceptionNet.

Table 6: Testing analysis of variation of DenseNet models with the proposed AB-SE-DenseNet model

Models	ACC	PR	RC	F1
DenseNet	85.60	87.37	85.13	86.12
SE - DenseNet - 1	92.15	93.38	92.43	92.88
SE - DenseNet - 2	94.05	94.22	95.79	94.99
SE - DenseNet - 3	95.58	96.12	95.53	95.77
AB - SE - DenseNet - 1	94.41	94.83	94.47	94.66
AB - SE - DenseNet - 2	98.58	98.69	98.53	98.61
AB - SE - DenseNet - 3	99.41	99.41	99.45	99.43

Table 6 and Figure 5 show the test results of changes in DenseNet designs. They highlight how adding different improvements affects them. The basic DenseNet model reaches an ACC of 85.60%. It has PRE, REC, and F1 at 87.37%, 85.13%, and 86.12%, respectively. Introducing Squeeze-and-Excitation (SE) modules consistently improves performance. SE-DenseNet-1 can reach an ACC of 92.15%. It also has good numbers for PRE, REC, and F1 at 93.38%, 92.43%, and 92.88%, respectively. The changes to SE-DenseNet-2 and SE-DenseNet-3 improve them. The ACCs for SE-DenseNet-2 and SE-DenseNet-3 are 94.05% and 95.58%, respectively. The PRE, REC, and F1s show that these improvements work well. Adding the Adaptive Bound (AB) to SE-DenseNet designs yields excellent results. AB-SE-DenseNet-1 gets 94.41% ACC. AB-SE-DenseNet-2 does much better at 98.58%. F1, PRE, and REC increased to 98.69%, 98.53%, and 98.61%, respectively. This shows better results with these models. The best model, AB-SE-DenseNet-3, reaches a fantastic 99.41% ACC. It has very good ACC, REC, and F1 scores. This shows that combining adaptive optimisation with squeezing-and-exciting designs significantly improves DenseNet performance.

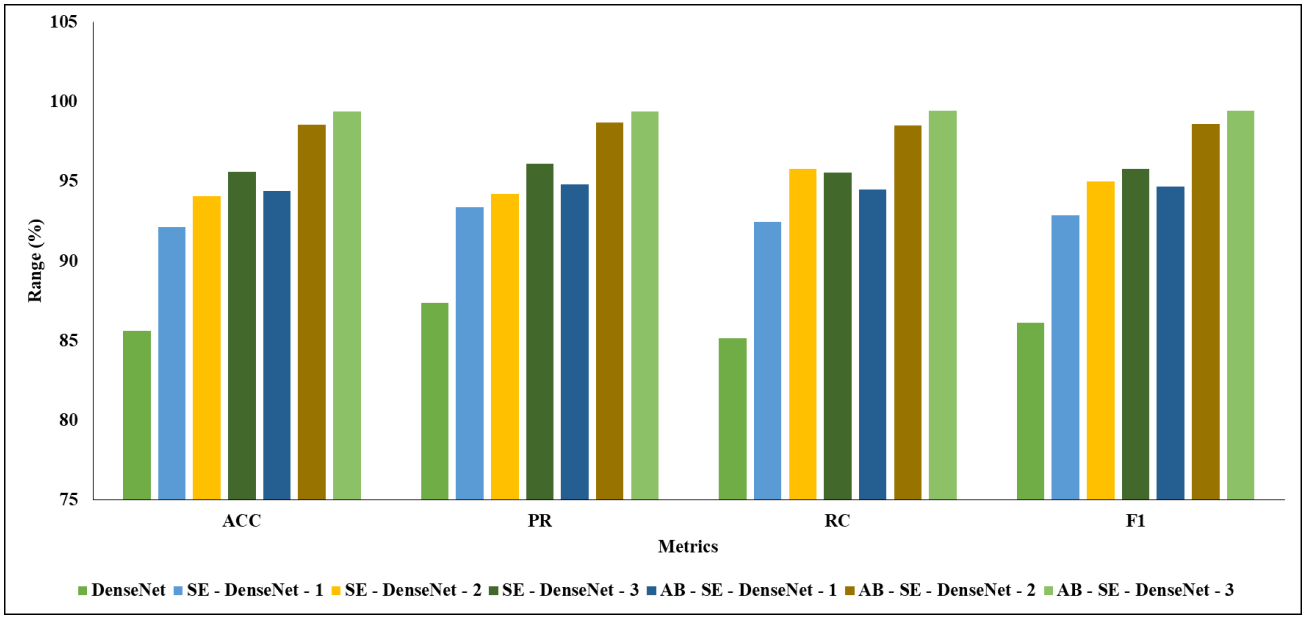

Figure 5: Variations of DenseNet models

5. Conclusion

In conclusion, this research introduces an innovative and comprehensive paradigm for cervical cancer detection that effectively addresses the enduring challenges of accuracy, robustness, and generality in current screening methods. The proposed method uses the publicly available SIPaKMeD dataset and combines advanced image preprocessing, deep feature extraction, and intelligent classification to provide highly reliable diagnostic results. In the preprocessing stage, Gabor filtering is used to extract texture patterns and structural details from cervical cell images. This makes the distinguishing features needed for accurate analysis stronger and lessens the effects of noise and other artefacts that aren't needed. A GhostNet-based architecture is used for feature extraction. It captures rich, informative representations while remaining efficient computationally. The Artificial Ecosystem Optimisation (AEO) technique is used to fine-tune hyperparameters to further improve the model's performance. This optimisation technique ensures balanced exploration and exploitation, leading to faster convergence, less overfitting, and better generalisation across datasets.

The proposed system presents an AdaBound-Squeeze-and-Excitation DenseNet (AB-SE-DenseNet) for classification, integrating adaptive optimisation via AdaBound with spatial squeeze-and-excitation processes. This hybrid architecture enables the model to adjust the learning rate and recalibrate channel-wise features on the fly, helping it focus on the most important features for detecting cervical cancer. This strengthens the categorisation process and improves its ability to detect subtle changes in cells that are important for early diagnosis. The proposed approach performs better than others, achieving 99.41% accuracy, 99.41% precision, 99.43% recall, and 99.45% F-score. The results clearly show that the AB-SE-DenseNet architecture outperforms the best existing methods and sets a new standard for diagnosing cervical cancer. Future research will focus on advancing this work through real-time system implementation, validation on larger, more heterogeneous datasets, and intensive engagement with medical specialists. These initiatives will make this framework much more useful in the clinic and accelerate the development of real, computer-aided diagnostic tools for cervical cancer screening.

Acknowledgement: The authors gratefully acknowledge New Horizon College of Engineering, Quest Technologies, Saranathan College of Engineering, and Chia Nan University of Pharmacy and Science for their valuable support and collaboration. Their collective contributions significantly strengthened the quality and outcomes of this research work.

Data Availability Statement: The data supporting the findings of this study are available from the corresponding author upon reasonable request.

Funding Statement: This research did not receive any external funding.

Conflicts of Interest Statement: The author declares that there are no conflicts of interest associated with this work.

Ethics and Consent Statement: Ethical approval was obtained, and informed consent was collected from both the organisation and all individual participants involved in the study.

References

1. V. Chandran, M. G. Sumithra, A. Karthick, T. George, M. Deivakani, B. Elakkiya, U. Subramaniam, and S. Manoharan, "Diagnosis of cervical cancer based on ensemble deep learning network using colposcopy images," *BioMed Research International*, vol. 2021, no. 5, pp. 1–15, 2021.
2. A. U. Rehman, N. Ali, I. A. Taj, M. Sajid, and K. S. Karimov, "An automatic mass screening system for cervical cancer detection based on convolutional neural network," *Mathematical Problems in Engineering*, vol. 2020, no. 10, pp. 1–14, 2020.
3. G. Kumawat, S. K. Vishwakarma, P. Chakrabarti, P. Chittora, T. Chakrabarti, and J. C. W. Lin, "Prognosis of cervical cancer disease by applying machine learning techniques," *Journal of Circuits, Systems and Computers*, vol. 32, no. 1, p. 2350019, 2023.
4. B. A. Mohammed, E. M. Senan, Z. G. Al-Mekhlafi, M. Alazmi, A. M. Alayba, A. A. Alanazi, A. Alreshidi, and M. Alshahrani, "Hybrid techniques for diagnosis with WSIs for early detection of cervical cancer based on fusion features," *Applied Sciences*, vol. 12, no. 17, pp. 1–23, 2022.
5. T. Dong, L. Wang, R. Li, Q. Liu, Y. Xu, Y. Wei, X. Jiao, X. Li, Y. Zhang, Y. Zhang, K. Song, X. Yang, and B. Cui, "Development of a novel deep learning-based prediction model for the prognosis of operable cervical cancer," *Computational and Mathematical Methods in Medicine*, vol. 2022, no. 14, pp. 1–14, 2022.
6. U. K. Lilhore, M. Poongodi, A. Kaur, S. Simaiya, A. D. Algarni, H. Elmannai, V. Vijayakumar, G. B. Tunze, and M. Hamdi, "Hybrid model for detection of cervical cancer using causal analysis and machine learning techniques," *Computational and Mathematical Methods in Medicine*, vol. 2022, no. 1, pp. 1–17, 2022.
7. S. Alsubai, A. Alqahtani, M. Sha, A. Almadhor, S. Abbas, H. Mughal, and M. Gregus, "Privacy preserved cervical cancer detection using convolutional neural networks applied to Pap smear images," *Computational and Mathematical Methods in Medicine*, vol. 2023, no. 1, pp. 1–8, 2023.
8. S. M. Abd-Alhalem, H. S. Marie, W. El-Shafai, T. Altameem, R. S. Rathore, and T. M. Hassan, "Cervical cancer classification based on a bilinear convolutional neural network approach and random projection," *Engineering Applications of Artificial Intelligence*, vol. 127, no. 1, p. 107261, 2024.
9. S. Cheng, S. Liu, J. Yu, G. Rao, Y. Xiao, W. Han, W. Zhu, X. Lv, N. Li, J. Cai, Z. Wang, X. Feng, F. Yang, X. Geng, J. Ma, X. Li, Z. Wei, X. Zhang, T. Quan, S. Zeng, L. Chen, J. Hu, and X. Liu, "Robust whole slide image analysis for cervical cancer screening using deep learning," *Nature Communications*, vol. 12, no. 1, pp. 1–10, 2021.
10. R. Gorantla, R. K. Singh, R. Pandey, and M. Jain, "Cervical cancer diagnosis using CervixNet – a deep learning approach," *in 2019 IEEE 19th International Conference on Bioinformatics and Bioengineering (BIBE)*, Athens, Greece, 2019.
11. V. S. Palanisamy, R. K. Athiappan, and T. Nagalingam, "Pap smear based cervical cancer detection using residual neural networks deep learning architecture," *Concurrency and Computation: Practice and Experience*, vol. 34, no. 4, p. e6608, 2022.
12. A. Tripathi, A. Arora, and A. Bhan, "Classification of cervical cancer using deep learning algorithm," *in 2021 5th International Conference on Intelligent Computing and Control Systems (ICICCS)*, Madurai, India, 2021.
13. O. Attallah, "Cervical cancer diagnosis based on multi-domain features using deep learning enhanced by handcrafted descriptors," *Applied Sciences*, vol. 13, no. 3, pp. 1–23, 2023.
14. S. Fekri-Ershad and M. F. Alsaffar, "Developing a tuned three-layer perceptron fed with trained deep convolutional neural networks for cervical cancer diagnosis," *Diagnostics*, vol. 13, no. 4, pp. 1–18, 2023.
15. H. Karamti, R. Alharthi, A. A. Anizi, R. M. Alhebshi, A. A. Eshmawi, S. Alsubai, and M. Umer, "Improving prediction of cervical cancer using KNN imputed SMOTE features and multi-model ensemble learning approach," *Cancers*, vol. 15, no. 17, pp. 1–19, 2023.
16. M. Alsalatie, H. Alquran, W. A. Mustafa, A. A. Zyout, A. M. Alqudah, R. Kaifi, and S. Qudsieh, "A new weighted deep learning feature using particle swarm and ant lion optimization for cervical cancer diagnosis on Pap smear images," *Diagnostics*, vol. 13, no. 17, pp. 1–19, 2023.
17. M. Hamdi, E. M. Senan, B. Awaji, F. Olayah, M. E. Jadhav, and K. M. Alalayah, "Analysis of WSI images by hybrid systems with fusion features for early diagnosis of cervical cancer," *Diagnostics*, vol. 13, no. 15, pp. 1–29, 2023.
18. M. Kalbhor, S. Shinde, D. E. Popescu, and D. J. Hemanth, "Hybridization of deep learning pre-trained models with machine learning classifiers and fuzzy min–max neural network for cervical cancer diagnosis," *Diagnostics*, vol. 13, no. 7, pp. 1–16, 2023.
19. R. Kavitha, D. K. Jothi, K. Saravanan, M. P. Swain, J. L. A. Gonzáles, R. J. Bhardwaj, and E. Adomako, "Ant colony optimization-enabled CNN deep learning technique for accurate detection of cervical cancer," *BioMed Research International*, vol. 2023, no. 4, pp. 1–9, 2023.
20. H. Alquran, M. Alsalatie, W. A. Mustafa, R. A. Abdi, and A. R. Ismail, "Cervical Net: A novel cervical cancer

classification using feature fusion," *Bioengineering*, vol. 9, no. 10, pp. 1–20, 2022.
21. P. Wang, Z. Wang, D. Lv, C. Zhang, and Y. Wang, "Low illumination color image enhancement based on Gabor filtering and Retinex theory," *Multimedia Tools and Applications*, vol. 80, no. 12, pp. 17705–17719, 2021.
22. H. P. Gandikota, "CT scan pancreatic cancer segmentation and classification using deep learning and the tunicate swarm algorithm," *PLOS ONE*, vol. 18, no. 11, pp. 1–16, 2023.
23. A. T. Sahlol, M. A. Elaziz, A. T. Jamal, R. Damaševičius, and O. F. Hassan, "A novel method for detection of tuberculosis in chest radiographs using artificial ecosystem-based optimisation of deep neural network features," *Symmetry*, vol. 12, no. 7, pp. 1–17, 2020.
24. W. Zhao, L. Wang, and Z. Zhang, "Artificial ecosystem-based optimization: A novel nature-inspired meta-heuristic algorithm," *Neural Computing and Applications*, vol. 32, no. 4, pp. 1–43, 2019.
25. M. Jiang, C. Feng, X. Fang, Q. Huang, C. Zhang, and X. Shi, "Rice disease identification method based on attention mechanism and deep dense network," *Electronics*, vol. 12, no. 3, pp. 1–14, 2023.